

Articles

An Experimentally Based Model of the Peroxidase-NADH Biochemical Oscillator: An Enzyme-Mediated Chemical Switch

Dean L. Olson, Erik P. Williksen, and Alexander Scheeline*

Contribution from the Department of Chemistry, University of Illinois at Urbana—Champaign, 600 S. Mathews Avenue, Urbana, Illinois 61801

Received August 1, 1994*

Abstract: The development of a chemically realistic model of the peroxidase-NADH biochemical oscillator is described, characterized, and compared with experiments. The selection of each reaction and rate constant in the model is chemically justified, and derived only from studies published by others, or our own laboratory data. Peroxidase and the modifier methylene blue are included in the model, along with correct incorporation of oxygen mass transport. No dimensionless or abstract variables were employed, and no specific attempt was made to include any principle of nonlinear dynamics commonly regarded as responsible for oscillations, such as autocatalysis, autoinhibition, or delayed feedback. Eight steps form the basis of a complete oscillation in the model, beginning with species initially present in experiments, and proceeding to a process dominated by the interconversion of native peroxidase (Per^{3+}) and Compound III (Cp III). Four additional steps relate directly to the conditions under which actual experiments were performed. Simulated numerical output is shown for all dynamical chemical species in a standard model. Results are similar to experimental data for oxygen, NADH, Per^{3+} , and Cp III. It is demonstrated in the model that oxygen growth and decay hinge on the reactivity of the superoxide radical ($\text{O}_2^{\cdot-}$). Two reactions operate as a chemical switch where Cp III serves as a regulatory intermediate. Oxidation of Per^{3+} to Cp III by reaction with $\text{O}_2^{\cdot-}$ occurs until Per^{3+} is depleted. Superoxide disproportion then becomes rate-limiting. The reaction rate of NAD^{\cdot} (a radical of nicotinamide adenine dinucleotide) with oxygen decreases for a short time. This allows NAD^{\cdot} to begin a cascade reaction to reduce Cp III back to Per^{3+} , which produces additional NAD^{\cdot} to rapidly consume remaining oxygen, replenish Per^{3+} , and initiate a new oscillation.

Introduction

Since its discovery in 1965,¹ to the present, at least 11 papers appeared which investigated the experimental aspects of the peroxidase-NADH oscillator.^{2–10} Theoretical considerations have been reported in no fewer than 19 studies, many of which were included in a recent review.¹¹ Variations on traditional experimental approaches to studying the oscillator have also appeared.^{12–15} While reasonable qualitative similarity has been achieved between some models and some experiments, quantitative agreement has proven elusive. In many cases, quantitative comparisons between models and experiments were not possible

because in simulated outputs, concentration and time had dimensionless units. Another reason for inadequate modeling has been a lack of published experimental rate constants for the steps in the models. In the model presented here, the most recent rate constant is from 1985 (a slightly revised value appeared in 1991). Yet, models have been proposed from as early as 1978.⁴ Inclusion of the enzyme in an oscillating numerical model did not appear until 1984.¹⁶ A further difficulty has been the inconsistent interpretation of the mass transport of oxygen between the liquid and gas phases, which is an integral part of the peroxidase-NADH oscillator. In addition to these practical problems, a fundamental principle of nonlinear dynamics comes into play in the transition of a system from stability to instability (oscillations). A result of universality is that many different models may have similar behavior near critical points. Consequently, a match between simulated and experimental data over a narrow range of conditions is not a very rigorous criterion of model validity. A better approach to model evaluation is whether the model contains known chemical reactions with measured rate constants, and whether simulations respond to numerical perturbations in a way similar to experimental results.

One overriding difficulty in understanding the peroxidase-NADH oscillator has been that existing models are not well-linked to actual experimental parameters. Most models do not seem to have been systematically developed using existing knowledge of reactions and rate constants from the literature.

- * Abstract published in *Advance ACS Abstracts*, December 1, 1994.
- (1) Yamazaki, I.; Yokota, K.; Nakajima, R. *Biochem. Biophys. Res. Commun.* **1965**, *21*, 582–586.
 - (2) Nakamura, S.; Yokota, K.; Yamazaki, I. *Nature* **1969**, *222*, 794.
 - (3) Olsen, L. F.; Degn, H. *Nature* **1977**, *267*, 177–178.
 - (4) Olsen, L. F.; Degn, H. *Biochim. Biophys. Acta* **1978**, *523*, 321–334.
 - (5) Geest, T.; Steinmetz, C. G.; Larter, R.; Olsen, L. F. *J. Phys. Chem.* **1992**, *96*, 5678–5680.
 - (6) Steinmetz, C. G.; Geest, T.; Larter, R. *J. Phys. Chem.* **1993**, *97*, 5649–5653.
 - (7) Watanabe, N.; Inaba, H. *Photochem. Photobiol.* **1993**, *57*, 570–576.
 - (8) Olson, D. L.; Scheeline, A. *Anal. Chim. Acta* **1993**, *283*, 703–717.
 - (9) Part 1: Olson, D. L.; Scheeline, A. *J. Phys. Chem.* in press.
 - (10) Part 2: Olson, D. L.; Scheeline, A. *J. Phys. Chem.* in press.
 - (11) Larter, R.; Olsen, L. F.; Steinmetz, C. G.; Geest, T. *Chaos in Chemistry and Biochemistry*; Field, R. J.; Györgyi, L., Eds.; World Scientific: London, 1993; Chapter 7.
 - (12) Lazar, J. G.; Ross, J. *Science* **1990**, *247*, 189–192.
 - (13) Lazar, J. G.; Ross, J. *J. Chem. Phys.* **1990**, *92*, 3579–3589.
 - (14) Samples, M. S.; Hung, Y.; Ross, J. *J. Phys. Chem.* **1992**, *96*, 7338–7342.
 - (15) Hauck, T.; Schneider, F. W. *J. Phys. Chem.* **1993**, *97*, 391–397.

- (16) Fed'kina, V. R.; Ataulakhanov, F. I.; Bronnikova, T. V. *Biophys. Chem.* **1984**, *19*, 259–264.

Model of the Peroxidase-NADH Oscillator

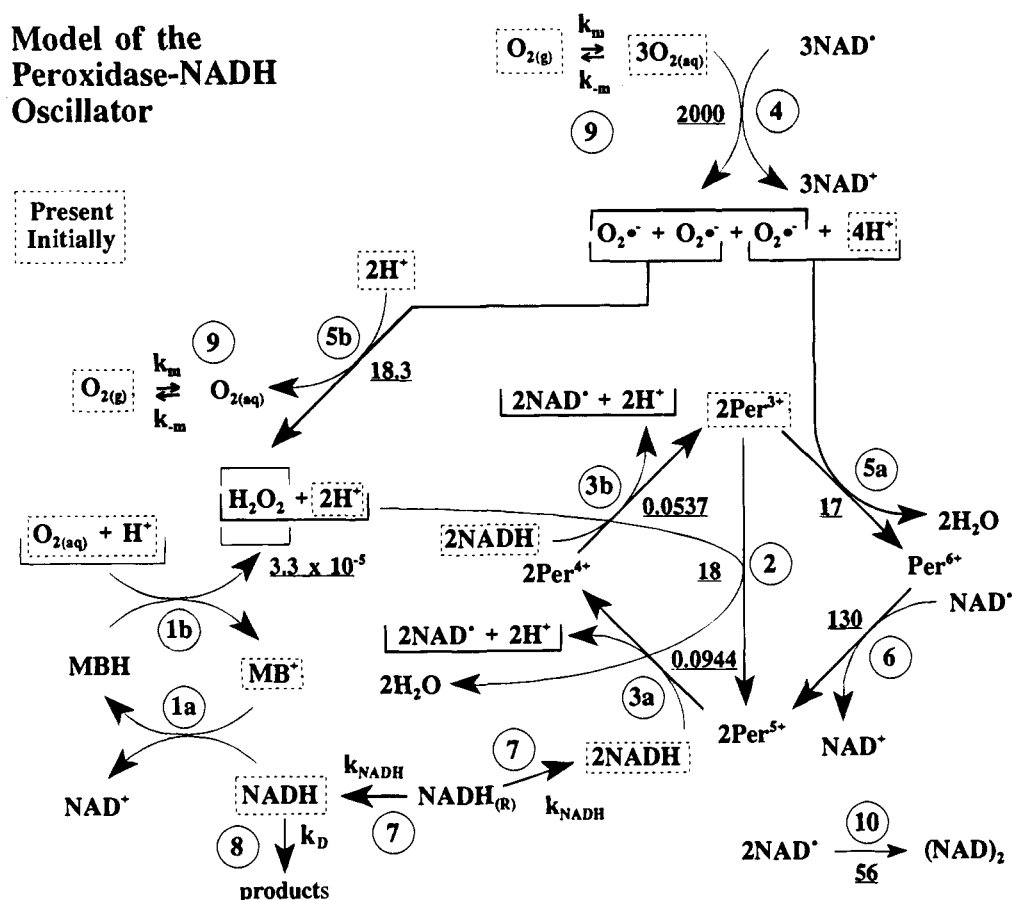


Figure 1. Standard Urbanalator model of the peroxidase-NADH oscillator. Circled numbers from 1–6 represent the apparent sequence of events which combine to form a cycle. Numbers 7–10 represent other reactions explained in the text. The underlined values are the corresponding rate constants (in $\mu M^{-1} s^{-1}$) from Table 2. The brackets represent the stoichiometry depicted in Table 1. Note that for clarity of presentation, the NAD^+ species are not linked by arrows.

Examples abound with improperly defined oxygen mass transport variables, several rate constants set to the same value, and scaled or dimensionless variables of poorly described utility. Previous research^{8–10} demonstrated that thorough characterization of apparatus and conditions is critical in defining an experimental procedure that will yield reproducible results toward the development of a realistic model. Because the model presented here is experimentally based, many aspects of the peroxidase-NADH oscillator are elucidated for the first time.

To date, no model has incorporated the modifiers 2,4-dichlorophenol (DCP) or oxidized methylene blue (MB^+), both traditionally included as standard ingredients of the oscillator. One significant difference between this work and that of many others is that this study does not use DCP, which has been claimed to prolong oscillations. We earlier showed that damped oscillations can be maintained for 6 h with added MB^+ only.⁸ The model introduced here includes all reactive chemical species initially present in our experiments, including MB^+ .

Work described in this paper sets out to start anew and build a working numerical model based on, and consistent with, experimental observations. The overall goal is to better explain how the oscillator works, and to develop a model which can serve as a guide to future experiments and further improvement of the model itself.

Experimental Section

Throughout this paper, the native horseradish peroxidase (HRP) enzyme used in experiments will be designated Per^{3+} . To highlight changes in oxidation states, HRP compounds II, I, and III will be designated Per^{4+} , Per^{5+} , and Per^{6+} , respectively.

Full descriptions of all laboratory procedures appear elsewhere,^{8–10} but they are summarized here. Oscillatory experiments were conducted under a set of standard conditions. The initial reaction solution is contained in a quartz cuvette and consists of 500 pyrogallol units/5 mL (about $7.9 \mu M$ HRP, based on the mass weighed and a molecular weight of 42 100 g/mol) and $0.2 \mu M$ methylene blue (MB^+) in 0.1 M sodium acetate buffer at pH 5.10. This mixture is deoxygenated by blowing 100% N_2 across the surface of the vigorously stirred solution. To measure the oxygen mass transport constant of $O_{2(aq)}$ out of solution, k_{-m} , the blanketing gas is changed to 1.50% $O_{2(g)}$ ($613 \mu M$ at 25 °C). The first-order oxygen growth data are acquired with a dissolved oxygen electrode and linearized to obtain k_{-m} . A typical experimental value is given in Table 2. The corresponding value for k_m is calculated using $K_{eq} = k_m/k_{-m} = 0.0292$.^{8,9} When oxygen equilibration is achieved, a reservoir solution of β -NADH at pH 7.00 is pressure-infused through a capillary at a slow flow rate which is matched to offset solution evaporation. After an induction period, oscillations commence. Four species are routinely monitored: $O_{2(aq)}$, Per^{3+} (wavelength of maximum absorbance at 402 nm), Per^{6+} (A_{418}), and NADH (A_{360}). A Hewlett-Packard ultraviolet–visible 8452A diode array spectrophotometer, with a wavelength resolution of 2 nm, was used for all absorbance measurements. Spectroscopic data shown here were taken under conditions of continuous illumination by the deuterium lamp in the instrument.⁹

The molar absorptivities of several compounds were determined for this study and used to convert absorbance data to concentration. All values were measured in the same buffer and pH used in oscillatory experiments. In the case of Per^{3+} and Per^{6+} , overlapping absorbances from oscillatory data were deconvolved and then converted to concentration by using Beer's law and solving the appropriate

Table 1. Main Reactions in Model and Overall Reaction

(1a)	$\text{NADH} + \text{MB}^+$	\longrightarrow	$\text{NAD}^+ + \text{MBH}$
(1b)	$\text{MBH} + \text{O}_2 + \text{H}^+$	\longrightarrow	$\text{MB}^+ + \text{H}_2\text{O}_2$
(2)	$\text{Per}^{3+} + \text{H}_2\text{O}_2 + 2\text{H}^+$	\longrightarrow	$\text{Per}^{5+} + 2\text{H}_2\text{O}$
(3a)	$2\text{Per}^{5+} + 2\text{NADH}$	\longrightarrow	$2\text{Per}^{4+} + 2\text{NAD}^+ + 2\text{H}^+$
(3b)	$2\text{Per}^{4+} + 2\text{NADH}$	\longrightarrow	$2\text{Per}^{3+} + 2\text{NAD}^+ + 2\text{H}^+$
(4)	$3\text{NAD}^+ + 3\text{O}_2$	\longrightarrow	$3\text{NAD}^+ + 3\text{O}_2^{\cdot-}$
(5a)	$\text{Per}^{3+} + \text{O}_2^{\cdot-} + 4\text{H}^+$	\longrightarrow	$\text{Per}^{6+} + 2\text{H}_2\text{O}$
(5b)	$2\text{O}_2^{\cdot-} + 2\text{H}^+$	\longrightarrow	$\text{H}_2\text{O}_2 + \text{O}_2$
(6)	$\text{Per}^{6+} + \text{NAD}^{\cdot}$	\longrightarrow	$\text{Per}^{5+} + \text{NAD}^+$
<hr/>			
Sum:	$5\text{NADH} + 3\text{O}_2 + 5\text{H}^+$	\longrightarrow	$5\text{NAD}^+ + \text{H}_2\text{O}_2 + 4\text{H}_2\text{O}$

simultaneous equations.¹⁷ The molar absorptivities (in units of $\text{M}^{-1}\text{cm}^{-1}$) are as follows: NADH , $\epsilon_{360} = 7800$; Per^{3+} , $\epsilon_{402} = 81900$ and $\epsilon_{418} = 45810$; Per^{6+} , $\epsilon_{418} = 87700$ and $\epsilon_{402} = 50120$. NADH was made up in pH 7 buffer, diluted into pH 5.10 buffer, and scanned immediately. Per^{6+} was made by mixing Per^{3+} with a 2000-fold molar excess of H_2O_2 ,¹⁸ it was scanned at once vs an identical solution containing only H_2O_2 . Some of the stated ϵ values are somewhat different from those reported elsewhere (Per^{3+} : 91000,¹⁹ 107700,²⁰ 102000,²¹ 100000,²² 101000,²³ Per^{6+} : 81000¹⁸). Independent measurements were made for the present study to ensure internal consistency with the pH, buffer, and commercial enzyme preparation used here.

Model Development

In the model depicted in Figure 1, the reactions are numbered in the sequence that they apparently occur to produce an oscillation. Reaction numbers including an "a" or "b" are conceptually linked. Brackets above and below the species indicate the balanced stoichiometry for the overall reaction scheme presented in Table 1. This particular stoichiometry is merely proposed as a reasonable possibility and has not been experimentally investigated. The net formation of H_2O_2 was intentionally included because of the observation that enzyme degradation occurs,^{8,9} perhaps via inactivation of the intermediate Per^{5+} by H_2O_2 .²⁴

Selection of Species and Reactions. The overriding principle behind development of the model was to use a minimum number of species and known reactions to yield simulated data that agree with experiments (ref 25, p 115). In general, reactions with the proper species were introduced in the order of occurrence that allows subsequent reactions to proceed. Once a sufficient number of reactions were added that all starting reactants are those initially present in an actual oscillatory

experiment, the model was considered nearly complete. (An additional step was added after failure analysis of the simulation indicated a high steady-state level of NAD^{\cdot} .) All but three of the model reactions have corresponding experimentally measured and published rate constants. Exceptions are justified below.

The process of building the model begins in Figure 1 at R_{5a} , which is based on the unambiguous spectroscopic observation that in a typical oscillation, the native enzyme, Per^{3+} , is slowly converted to Per^{6+} and then quickly back to Per^{3+} .⁸ This is evidenced by monitoring absorbance at 402 and 418 nm for Per^{3+} and Per^{6+} , respectively, in a working oscillator as illustrated previously.^{8,9} Data deconvolved using the four molar absorptivities mentioned earlier and applied to previous experiments done under standard conditions of continuous illumination⁸ are shown in Figure 2a and strongly suggest a clean, nearly unimolecular interconversion between Per^{3+} and Per^{6+} . The molar sum of the two species shown in the top trace of Figure 2a accounts for most, but not all, of the oscillatory behavior observed at those wavelengths. Absorbance of enzyme intermediates and other species (such as $(\text{NAD})_2$)^{26,27} or inaccuracies in the measured molar absorptivities could be the source of the variation in the calculated sum of $[\text{Per}^{3+}] + [\text{Per}^{6+}]$. In addition, the corresponding phase portrait in Figure 2b indicates virtually no side reactions or spectroscopically evident intermediates. The damping of oscillatory amplitude, due to a presently undetermined enzyme degradation process, is clearly evident in both parts of Figure 2.

A portion of a similar data set of about 1.5 oscillations is presented three-dimensionally in the upper portion of Figure 3. Moving parallel to the time axis, an absorbance increase indicates production of an absorbing species, and a decrease indicates consumption. The chosen region from 450 to 700 nm is distinctive in identifying HRP oxidation states.²⁸ The first feature to point out in Figure 3 is the isosbestic wavelength for Per^{3+} and Per^{6+} , 462 nm.²² If only Per^{3+} and Per^{6+} absorb in this region, and these two species cleanly and completely interconvert, the absorbance at the isosbestic wavelength will be constant over time. The variation in A_{462} compared to other absorbance changes in the shown region is less than 8.6%, indicating that the isosbestic behavior at 462 nm is fairly good. Also, the profile of absorbance vs time at 460 and 464 nm, the wavelengths on each side of the isosbestic wavelength, is opposite in appearance across the course of an oscillation. At 460 nm, the absorbance first increases, then decreases, but at 464 nm, it decreases, then increases. To further explore which enzyme species may be present, the peaks and troughs in the region of 450–700 nm can be compared to the known wavelengths of absorbance for Per^{3+} and Per^{6+} . Per^{3+} has local absorbance maxima at 496 nm and 638 nm. Per^{6+} has local maxima at 544 and 578 nm. The two troughs which begin at $t = 0$ in Figure 3 occur at precisely the wavelengths characteristic of Per^{3+} , suggesting Per^{3+} consumption. Of the two peaks at 548 and 578 nm, the latter is an exact match for Per^{6+} , and the former is high by just 4 nm from the other local maximum for Per^{6+} . The relative heights of A_{548} and A_{578} are reversed from that of a spectrum of Per^{6+} alone. The smaller than expected height of A_{548} and the slight shift of its location to a higher wavelength are consistent with A_{548} being convolved with the absorbance of Per^{3+} on a broad shoulder as Per^{3+}

(17) Harris, D. C. *Quantitative Chemical Analysis*, 3rd ed.; W. H. Freeman: New York, 1991.

(18) George, P. J. *Biol. Chem.* **1953**, *201*, 427–434.

(19) Keilin, D.; Hartree, E. F. *Biochem. J.* **1951**, *49*, 88–104.

(20) Paul, K. G. *The Enzyme*; Boyer, P. D., Lardy, H., Myrback, K., Eds.; Academic Press: New York, 1963; Vol. 8.

(21) Schonbaum, G. R.; Lo, S. J. *Biol. Chem.* **1972**, *247*, 3353–3360.

(22) Yamazaki, H.; Yamazaki, I. *Arch. Biochem. Biophys.* **1973**, *154*, 147–159.

(23) Cass, A. E.; Smit, M. H. *Trends in Electrochemical Biosensors*; Costa, G., Miertus, S., Eds.; World Scientific: New Jersey, 1992.

(24) Arnao, M. B.; Acosta, M.; del Rio, J. A.; Varon, R.; Garcia-Canovas, F. *Biochim. Biophys. Acta* **1990**, *1041*, 43–47.

(25) Connors, K. A. *Chemical Kinetics: The Study of Reaction Rates in Solution*; VCH: New York, 1990; Chapter 3.

(26) Burnett, R. W.; Underwood, A. L. *Biochemistry* **1968**, *7*, 3328–3333.

(27) Land, E. J.; Swallow, A. J. *Biochim. Biophys. Acta* **1968**, *162*, 327–337.

(28) Yamazaki, I.; Piette, L. H. *Biochim. Biophys. Acta* **1963**, *77*, 47–64.

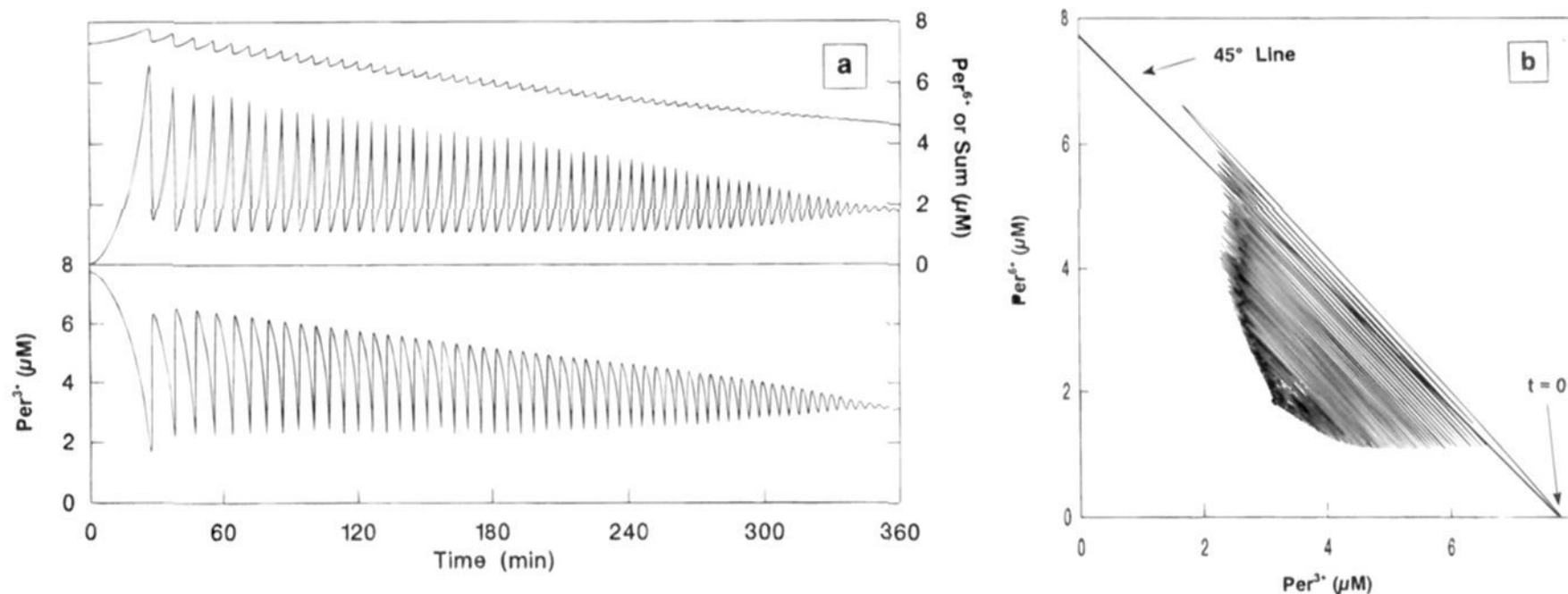


Figure 2. (a) Deconvoluted spectroscopic enzyme data from a standard oscillatory experiment. Per^{3+} and Per^{6+} were both monitored at 402 and 418 nm under standard conditions (raw data in ref 8). Molar absorptivities used for deconvolution appear in the Experimental Section. The two concentrations were summed to get the trace shown at the top. Data are at 10 s intervals. (b) Phase portrait of the deconvoluted enzyme data in 2a. A phase response like the idealized 45° line shown would indicate complete, unimolecular, and undamped interconversion between two species. The interconversion between Per^{3+} and Per^{6+} is nearly, but clearly not quite, ideal. Time could be indicated by tic marks along the lines (omitted for clarity). All 6 h of data from (a) are shown.

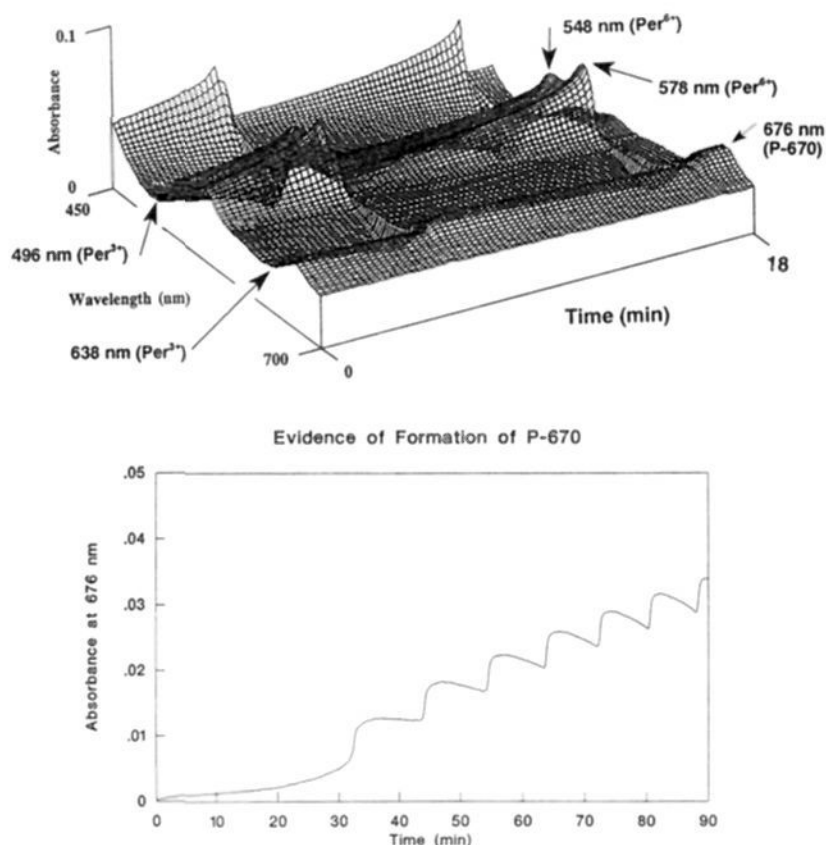


Figure 3. Three-dimensional presentation of spectroscopic oscillatory data. Absorbance vs wavelength data are shown in the upper figure at 10 s intervals for a region including about 1.5 oscillations taken under standard experimental conditions.⁸ Marked features are discussed in the text. The lower plot shows the increase, over several oscillations, in A_{676} , which corresponds to the formation of the compound P-670 at pH 5.

decreases. As the level of Per^{3+} goes down, A_{548} , corresponding to Per^{6+} , is smaller than expected and shifted away from the falling shoulder of absorbance due to Per^{3+} .

One other distinguishable feature is seen in Figure 3. Though not readily evident as shown in the 3-dimensional data, when viewed in cross-section as absorbance vs time, A_{676} increases with each successive oscillation as seen in the lower plot. This absorbance nearly matches that for the formation of compound P-670 at pH 5 in acetate buffer.²² P-670 is an inactive form of HRP and forms irreversibly from attack of Per^{5+} by H_2O_2 .^{24,29}

The relatively constant absorbance at the isosbestic wavelength and the absorbance changes at the peaks and troughs in Figure 3 support the earlier suggestion that Per^{3+} and Per^{6+} are the only enzyme oxidation states significantly present and that their interconversion does not reveal spectroscopically distinguishable intermediates under these conditions.

The next species added to the model, superoxide ($\text{O}_2^{\bullet-}$), allows the conversion of $\text{Per}^{3+} \rightarrow \text{Per}^{6+}$ via the known R_{5a} , which is not directly reversible. It is well established³⁰ that Per^{6+} must pass through each lower oxidation level to return to Per^{3+} . (Data in Figures 2 and 3 would indicate that these intermediates are short-lived.) To continue building the model, it is recognized that the addition of $\text{O}_2^{\bullet-}$ requires a known reaction which yields $\text{O}_2^{\bullet-}$ as a product, such as the reaction of NAD^\bullet with oxygen (R_4). Also, $\text{O}_2^{\bullet-}$ will react with H^+ (always present since experimental pH is 5.10) to form H_2O_2 and $\text{O}_{2(aq)}$ (R_{5b}). In turn, H_2O_2 can oxidize Per^{3+} to Per^{5+} (R_2). The Per^{5+} can react with the NADH initially present to form Per^{4+} and NAD^\bullet (R_{3a}). Per^{4+} reacts similarly with NADH forming Per^{3+} and more NAD^\bullet (R_{3b}). NAD^\bullet can reduce Per^{6+} to Per^{5+} (R_6).

R_6 , R_{3a} , and R_{3b} complete the basic cycle required for the interconversion of Per^{3+} and Per^{6+} . An initial source of H_2O_2 is required for $\text{Per}^{3+} \rightarrow \text{Per}^{5+}$, which initiates the formation of NAD^\bullet . In the model, H_2O_2 originates from the MB^+ -catalyzed oxidation of NADH by oxygen.³¹ The addition of forward and reverse oxygen mass transport expressions (R_9), constant feed of NADH from a reservoir (R_7), and known degradation⁸ of NADH at pH 5.10 nearly complete the construction of the model.

Reactions 1–6 (a total of 8 steps) form the basis of a complete cycle, beginning with species present initially and proceeding to a process highlighted by the interconversion of Per^{3+} and Per^{6+} . Reactions 7–9 relate to the conditions under which actual experiments are performed.

Three known reactions should be discussed that were not included in the model up to this point. They are³²

(30) Dunford, H. B. *Peroxidases in Chemistry and Biology*; Everse, J., Everse, K. E., Grisham, M. B., Eds.; CRC Press: Ann Arbor, 1991; Vol. 2, pp 1–24.

(31) Sevcik, P.; Dunford, H. B. *J. Phys. Chem.* **1991**, *95*, 2411–2415.

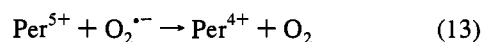
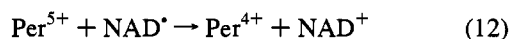
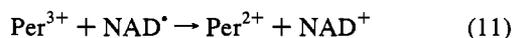
(32) Kobayashi, K.; Hayashi, K.; Swallow, A. J. *Biochemistry* **1990**, *29*, 2080–2084.

(29) Bagger, S.; Williams, R. J. *Acta Chem. Scand.* **1971**, *25*, 976–982.

Table 2. List of Critical Rate Constants in the Urbanalator Model of the Peroxidase-NADH Oscillator

	reaction	rate constant	pH	ref
R ₁	NADH + O _{2(aq)} + H ⁺ → NAD ⁺ + H ₂ O ₂	k ₁ = 33 M ⁻¹ s ⁻¹ = 34 M ⁻¹ s ⁻¹	(5.1) ^{a,b}	31 33
R ₂	Per ³⁺ + H ₂ O ₂ + 2H ⁺ → Per ⁵⁺ + 2H ₂ O	k ₂ = 1.8 × 10 ⁷ M ⁻¹ s ⁻¹ = 0.9 × 10 ⁷ M ⁻¹ s ⁻¹	7.0 4.7	60 61
R _{3a}	Per ⁵⁺ + NADH → Per ⁴⁺ + NAD [•] + H ⁺	k _{3a} = 9.44 × 10 ⁴ M ⁻¹ s ⁻¹ = 5.4 × 10 ³ M ⁻¹ s ⁻¹	(5.1) ^a 5.6	62 35
R _{3b}	Per ⁴⁺ + NADH → Per ³⁺ + NAD [•] + H ⁺	k _{3b} = 5.37 × 10 ⁴ M ⁻¹ s ⁻¹ = 8.0 × 10 ² M ⁻¹ s ⁻¹	(5.1) ^a 5.6	62 35
R ₄	NAD [•] + O _{2(aq)} → NAD ⁺ + O _{2^{•-}}	k ₄ = 2.0 × 10 ⁹ M ⁻¹ s ⁻¹	8.6	63
R _{5a}	Per ³⁺ + O _{2^{•-}} + 4H ⁺ → Per ⁶⁺ + 2H ₂ O	k _{5a} = (3.4–35) × 10 ⁷ M ⁻¹ s ⁻¹ = 1.7 × 10 ⁷ M ⁻¹ s ⁻¹ (used) = 1.5 × 10 ⁵ M ⁻¹ s ⁻¹	5.0 5.1	64 65
R _{5b}	2O _{2^{•-}} + 2H ⁺ → H ₂ O ₂ + O _{2(aq)}	k _{5b} = 1.83 × 10 ⁷ M ⁻¹ s ⁻¹ = 2 × 10 ⁷ M ⁻¹ s ⁻¹	5.16 (5.1) ^a	66 67
R ₆	Per ⁶⁺ + NAD [•] → Per ⁵⁺ + NAD ⁺	k ₆ = 1.3 × 10 ⁸ M ⁻¹ s ⁻¹	(5.6) ^c	35
R ₇	NADH _R → NADH	k _{NADH} = 1.72 × 10 ⁻⁵ s ⁻¹	5.10	8
R ₈	NADH → NADH _p (products)	k _{D,0.1} = 5.56 × 10 ⁻⁵ s ⁻¹	5.10	8
R _{9a}	O _{2(g)} → O _{2(aq)}	k _m = 0.0044 min ⁻¹ = 7.30 × 10 ⁻⁵ s ⁻¹	5.10	9
R _{9b}	O _{2(aq)} → O _{2(g)}	k _{-m} = 0.150 min ⁻¹ = 2.50 × 10 ⁻³ s ⁻¹	5.10	9
R ₁₀	2NAD [•] → (NAD) ₂	k ₁₀ = 5.6 × 10 ⁷ M ⁻¹ s ⁻¹	6.4	27

^a Computed for pH 5.1 from data and expressions in the cited article. ^b Computed: pH 5.1, 0.2 μM MB⁺. ^c From computer fit.



For these reactions, the given corresponding rate constants (M⁻¹ s⁻¹) at pH 7.0 are k₁₁ = 8 × 10⁸, k₁₂ = 1.5 × 10⁸, and k₁₃ = 1.6 × 10⁶. In consideration of R₁₁, no spectroscopic evidence was seen for the formation of Per²⁺ (ferroperoxidase). Since no compelling reason exists to require its formation, it was not added to the model at this time. In regard to R₁₂, once Per⁵⁺ is formed from Per³⁺ and H₂O₂, NAD[•] has not yet formed. Though R₁₂ could presumably occur subsequently, NADH is already present in relatively high concentration, so NAD[•] is not needed to transform Per⁵⁺ to Per⁴⁺. Again, for the sake of simplicity, R₁₂ was omitted. Similarly, for R₁₃, when Per⁵⁺ is first formed, O_{2^{•-}} does not yet exist (it is made by NAD[•] and O_{2(aq)} in R₄). The NADH concentration will be relatively high to accomplish the reduction of Per⁵⁺, so R₁₃ was excluded from the model at this time. No absolute basis exists to eliminate reactions 11–13 from the model. For no other reason than to construct the simplest possible, minimal model, these reactions were not included. They will be considered in future research and refinement of the preliminary model developed here.

Selection of Rate Constants. Table 2 summarizes the rate constants used in the model presented in Figure 1. All but three of the rate constants were directly measured experimentally in the cited reference. For R₁, k₁ was computed using an expression derived from³¹

$$\frac{-d[\text{NADH}]}{dt} = k_{\text{obs}}[\text{NADH}] \quad (\text{R}_{1c})$$

where k_{obs} = k[MB⁺][O₂][H⁺] = 5.18 × 10⁻⁵ s⁻¹ and in the conditions described: [MB⁺] = 9.95 μM, [O₂] = 249 μM, at pH 9.0. This yields k = 2.09 × 10¹³ M⁻³ s⁻¹. If k₁ = k[MB⁺][H⁺] for standard oscillatory experimental conditions (0.2 μM MB⁺, pH 5.10), which assumes the degradation of NADH is first order in MB⁺, H⁺, and O₂, the computed value for k₁ is 33 M⁻¹ s⁻¹, as listed on Table 2. The value of k_{obs}

used above agrees closely with other work.³³ The first-order dependence of k_{obs} on MB⁺ was demonstrated at pH 9,^{31,34} but the first-order behavior of O₂ and H⁺ in R₁ has not been explored and is merely assumed in this computation. It should be noted that kinetic data for the MB⁺-catalyzed oxidation of NADH below pH 8 are not in the literature. A linear extrapolation of three existing data points from pH 8–9³⁴ yields a negative rate constant for pH 5.1. Though such an extrapolation is hardly reasonable, the result calls into question the assumptions made in the calculation of k₁ above. Consequently, the value of k₁ in Table 2 must be considered tentative.

The rate constant for R₆ was computed by fitting simulated, non-oscillatory data to similar experimental data.³⁵ For R_{5a}, only an order of magnitude range is available for the rate constant. Initially, the midpoint of the range was used, which was later slightly adjusted to yield simulations that were a better match to experimental oscillatory data. This is described more fully in the next section. All other rate constants are either derived directly from our own experiments or cited from the literature, as indicated. For R₃, k₃ is for conditions of continuous illumination.⁸ Rate constants listed as second entries for a given reaction in Table 2 are included only for comparison but are not judged to be the best values available. Use of these secondary values in the model has not been explored here. The model proposed here is structurally similar to some previous attempts.^{16,36–37} One major difference is the use of experimentally derived rate constants. Other distinct differences include the complete and consistent description of oxygen mass transport and the inclusion of (NAD)₂ formation from NAD[•].

Characterization of the Numerical Model. A program for integration of reaction rate equations named HAVCHM^{38,39} was obtained from Project Seraphim (Madison, WI). The program runs on any IBM computer or compatible, is written in Turbo Pascal version 3.0, and computes in double precision variables.

(33) Lee, L. G.; Whitesides, G. M. *J. Am. Chem. Soc.* **1985**, *107*, 6999–7008.

(34) Williams, D. C., III; Seitz, W. R. *Anal. Chem.* **1976**, *48*, 1478–1481.

(35) Yokota, K.; Yamazaki, I. *Biochemistry* **1977**, *16*, 1913–1920.

(36) Aguda, B. D.; Larter, R. *J. Am. Chem. Soc.* **1991**, *113*, 7913–7916.

(37) Fed'kina, V. R.; Bronnikova, T. V.; Ataullakhanov, F. I. *Biophysics* **1992**, *37*, 781–789.

(38) Chesick, J. P. *J. Chem. Educ.* **1988**, *65*, 599–602.

(39) Stabler, R. N.; Chesick, J. P. *Int. Chem. Kinet.* **1978**, *10*, 461–469.

Table 3. Rate Expressions Used in the Urbanator Model of the Peroxidase-NADH Oscillator

$$\begin{aligned}
 \text{(a)} \quad & d[\text{NADH}]/dt = -k_1[\text{NADH}][\text{O}_2]_{\text{aq}} - k_{3a}[\text{NADH}][\text{Per}^{5+}] - k_{3b}[\text{NADH}][\text{Per}^{4+}] + k_7[\text{NADH}]_R - k_8[\text{NADH}] \\
 \text{(b)} \quad & d[\text{O}_2]_{\text{aq}}/dt = -k_1[\text{NADH}][\text{O}_2]_{\text{aq}} - k_4[\text{NAD}^*][\text{O}_2]_{\text{aq}} + k_{5b}[\text{O}_2^{*-}]^2 + k_{9a}[\text{O}_2]_g - k_{9b}[\text{O}_2]_{\text{aq}} \\
 \text{(c)} \quad & d[\text{NAD}^*]/dt = k_{3a}[\text{Per}^{5+}][\text{NADH}] + k_{3b}[\text{Per}^{4+}][\text{NADH}] - k_4[\text{NAD}^*][\text{O}_2]_{\text{aq}} - k_6[\text{Per}^{6+}][\text{NAD}^*] - 2k_{10}[\text{NAD}^*]^2 \\
 \text{(d)} \quad & d[\text{Per}^{3+}]/dt = -k_2[\text{Per}^{3+}][\text{H}_2\text{O}_2] + k_{3b}[\text{Per}^{4+}][\text{NADH}] - k_{5a}[\text{Per}^{3+}][\text{O}_2^{*-}] \\
 \text{(e)} \quad & d[\text{Per}^{4+}]/dt = k_{3a}[\text{Per}^{5+}][\text{NADH}] - k_{3b}[\text{Per}^{4+}][\text{NADH}] \\
 \text{(f)} \quad & d[\text{Per}^{5+}]/dt = k_2[\text{Per}^{3+}][\text{H}_2\text{O}_2] - k_{3a}[\text{Per}^{5+}][\text{NADH}] + k_6[\text{Per}^{6+}][\text{NAD}^*] \\
 \text{(g)} \quad & d[\text{Per}^{6+}]/dt = k_{5a}[\text{Per}^{3+}][\text{O}_2^{*-}] - k_6[\text{Per}^{6+}][\text{NAD}^*] \\
 \text{(h)} \quad & d[\text{H}_2\text{O}_2]/dt = k_1[\text{NADH}][\text{O}_2]_{\text{aq}} - k_2[\text{Per}^{3+}][\text{H}_2\text{O}_2] + k_{5b}[\text{O}_2^{*-}]^2 \\
 \text{(i)} \quad & d[\text{O}_2^{*-}]/dt = k_4[\text{NAD}^*][\text{O}_2]_{\text{aq}} - k_{5a}[\text{Per}^{3+}][\text{O}_2^{*-}] - 2k_{5b}[\text{O}_2^{*-}]^2 \\
 \text{(j)} \quad & d[(\text{NAD})_2]/dt = k_{10}[\text{NAD}^*]^2
 \end{aligned}$$

Initial Conditions: $[\text{Per}^{3+}] = 7.9 \mu\text{M}$
 $[\text{O}_2]_{\text{aq}} = 17.9 \mu\text{M}$
 $[\text{O}_2]_g = 613 \mu\text{M}$ (fixed)
 $[\text{NADH}]_R = 6370 \mu\text{M}$ (fixed)
 all other initial concentrations are zero
 step error = 1×10^{-3}

The source code was obtained by special request and slightly modified to create ASCII data sets for import by a spreadsheet. The program is interactive and provides easy creating and editing of reaction parameter sets including reactions, rate constants, initial conditions, and designation of fixed concentrations. HAVCHM uses the Gear integration routine;⁴⁰ the fitting error is specified by the user and minimized by trial and error. Specification of a non-zero integration step interval yields output unevenly spaced in time. Setting of the step interval to zero allows linearly interpolated output evenly spaced in a chosen time interval. This feature provides evenly spaced data for comparison to other simulated or experimental data using a spreadsheet. Unless otherwise indicated, the time interval was set to 10 s to match experimental data.

For convenience, the rate constants on Table 2 were converted to units of $\mu\text{M}^{-1} \text{s}^{-1}$, and these values appear beside the appropriate reaction in Figure 1. The resultant HAVCHM output will be concentration in μM vs time in s. No parameters are dimensionless nor scaled in any way. The initial conditions are $[\text{Per}^{3+}] = 7.9 \mu\text{M}$, $[\text{O}_2]_{\text{aq}} = 17.9 \mu\text{M}$, $[\text{NADH}]_R = 6370 \mu\text{M}$ (the fixed reservoir concentration of NADH), and $[\text{O}_2]_g = 613 \mu\text{M}$, also fixed and derived from the 1.50% O_2 blown across the surface of the liquid in the reaction cuvette. All other initial concentrations are zero and all of these specifications represent standard experimental conditions.⁸ The reader is cautioned that H^+ does not appear in any of the rate expressions that accompany the rate constants in Table 2. In addition, it is advisable to fix the concentrations of NAD^+ , H_2O , and NADH to speed integration since these species are unreactive products. However, if not fixed, these species can serve as dummy tracers for the corresponding reactions; similar dummy species can be created to monitor other reactions if desired. The typical HAVCHM fitting error was set at 1×10^{-3} . If a smaller error setting is used, the program behaves erratically or terminates. A larger setting results in mass balance violations in Per^{3+} and Per^{6+} . On an IBM computer with a 486 co-processor operating at 66 MHz, a typical set of model parameters produces 2 h of numerical data in <1 min.

For $k_{5a} = 192 \mu\text{M}^{-1} \text{s}^{-1}$, the midpoint of the given range on Table 2, the numerically simulated oxygen output appears in Figure 4a. The system achieves a steady state in most species in about 13 min. Per^{3+} is seen to be converted to Per^{6+} accompanied by $\text{O}_{2(\text{aq})}$ consumption and NADH influx. At 13 min, NAD^* suddenly jumps from virtually zero to about $18 \mu\text{M}$, where it remains. O_2 and Per^{6+} are then suppressed near zero, and Per^{3+} is steady at its original concentration. Inspection of

Figure 1 leads to the conclusion that R_4 and R_6 become dominant, causing complete O_2 and Per^{6+} depletion. Even though R_{3a} and R_{3b} have relatively small rate constants, the $[\text{NADH}]$ is suppressed from a high concentration of over $50 \mu\text{M}$, which apparently causes R_{3a} and R_{3b} to go fast, thus maintaining Per^{3+} high.

To decrease the level of NAD^* radical present, an additional reaction was added to the model: the dimerization of 2NAD^* to $(\text{NAD})_2$. This reaction and its corresponding rate constant appear in Table 2. Inclusion of this reaction in the overall stoichiometry would significantly alter the relatively simple scheme presented in Table 1. A revised stoichiometry is proposed elsewhere,⁴¹ and only the simpler scheme is depicted in Figure 1. The numerically simulated oxygen output from the model for $k_{5a} = 192 \mu\text{M}^{-1} \text{s}^{-1}$ (the midpoint of the given range on Table 2), and now including NAD^* dimerization (R_{10}), is seen to oscillate. The result is presented in Figure 4b. Though allowance for $(\text{NAD})_2$ formation has yielded oscillations, the oxygen peaks are not well-rounded like those observed in experiments.⁸ Upon inspection of Figure 1, it was thought that R_{5a} might be too fast, causing a pronounced consumption of oxygen before a well-rounded peak is formed. Note that R_{5a} is a net oxygen consumer when linked to R_4 . Consequently, k_{5a} was decreased to the lower limit of its range, $34 \mu\text{M}^{-1} \text{s}^{-1}$, with the result presented as the middle trace in Figure 4b. A small irregularity still remains as a spike on the falling side of the peak, so k_{5a} was decreased a minimum additional amount to yield the results presented in the lower portion of Figure 4b, which are very similar in overall appearance to experimental data. The final value of k_{5a} was $17 \mu\text{M}^{-1} \text{s}^{-1}$, half the lower limit from the literature. This value appears in Figure 1 and on Table 2. It is the only rate constant in the model not computed or directly derived from experiment.

The shoulder seen on the oxygen traces in Figure 4b, well before the first minimum, is never seen in successful experimental runs. The shoulder becomes smaller as k_{5a} decreases in the model, and its meaning is unknown. Under certain experimental conditions which do not result in oscillations (too little enzyme, no MB^+ included, and others),⁴¹ the failure can often be predicted. Instead of the $\text{O}_{2(\text{aq})}$ steadily decreasing (as in Figure 5), the oxygen trace reaches a point about at the location of the shoulders in Figure 4b and then goes through an inflection point before reaching a non-zero steady state. The relation between these two observations remains unexplained, but it seems odd that they occur at about the same place in both experimental and numerical runs.

(40) Gear, C. W. *Numerical Initial Value Problems in Ordinary Differential Equations*; Prentice-Hall: Englewood Cliffs, New Jersey, 1971.

(41) Olson, D. L. Ph.D. Thesis, University of Illinois: Urbana, IL, 1994.

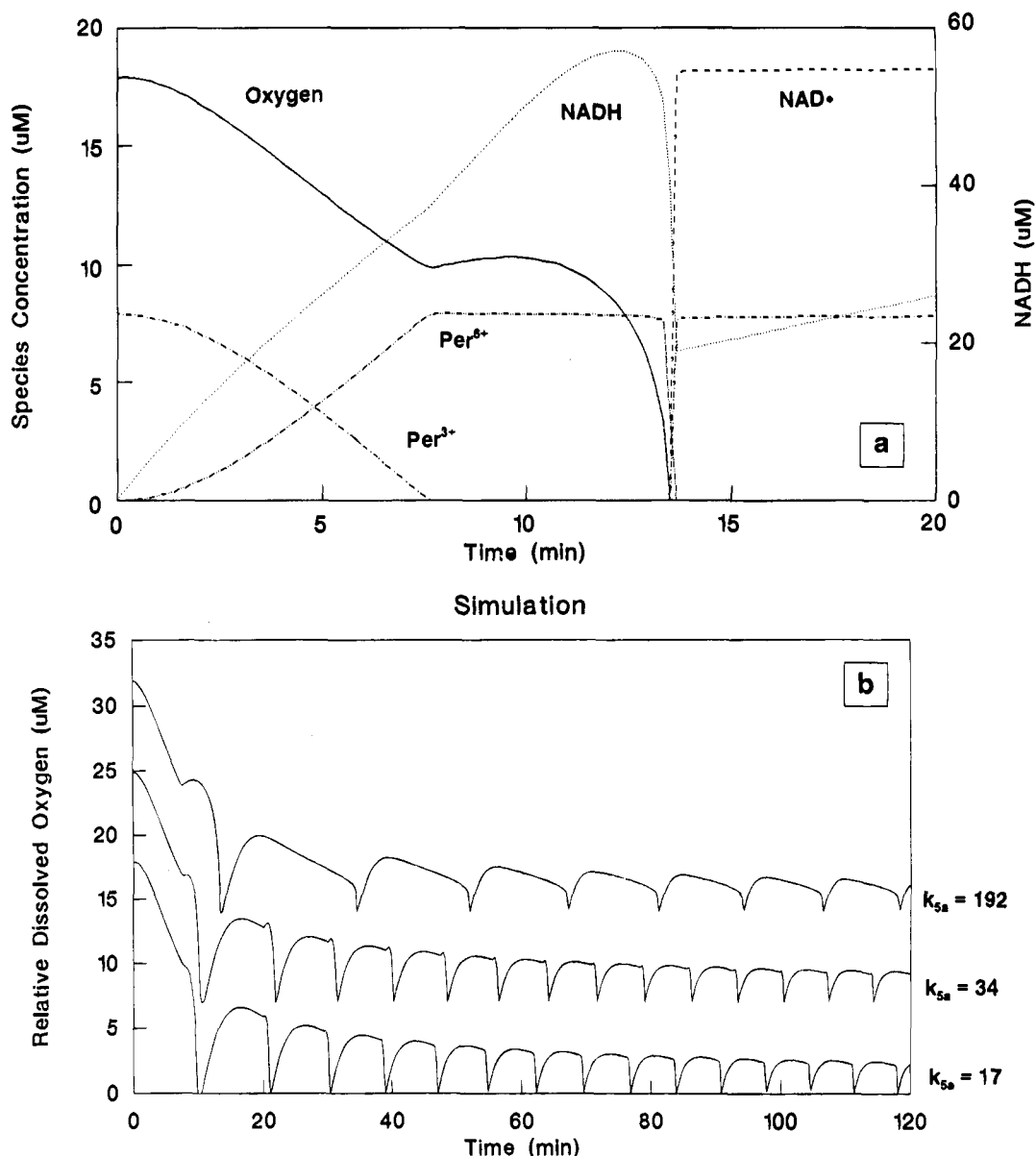


Figure 4. (a) Simulated data from the model, but with omission of R_{10} . Other conditions are included in Tables 2 and 3 and depicted in Figure 1. Except for the linear increase in NADH, all species shown remain at a steady state after about 13 min. (b) Effect on simulated data of including R_{10} and varying k_{5a} . All conditions appear in Tables 2 and 3. From top to bottom, the three values used for k_{5a} are the midpoint of its range in the literature, the lower range, and half its lower range. The two upper traces are offset for clarity of presentation.

We have named the final, standard model the *Urbanalator*, after where the work was done. As presented in Figure 1 and Table 2, it consists of 13 reactions and rate constants, 15 species, and 4 non-zero initial concentrations. Nine of the rate constants are from the literature, and four are from our own experiments.⁸ Four of the product species are unreactive and are omitted in numerical computations. This results in a total of 28 chemical specifications to be entered into the numerical integration routine. All included reactions derive from support of the interconversion of Per^{3+} and Per^{6+} , except for the inclusion of $(\text{NAD})_2$ formation, which was deemed necessary by analysis of oscillatory failure when it was omitted. The value for k_1 was computed here using tentative assumptions in the absence of experimental data at the standard oscillator pH of 5.10. The value of k_6 was found by others via computer fitting. Only k_{5a} was slightly adjusted to provide fine tuning of the simulated oxygen data to match its appearance with that from experiments.

The differential equations corresponding to the reactions in Table 2 appear in Table 3. Each reactive, non-constant species has a rate expression, which means nine corresponding dif-

ferential equations. $(\text{NAD})_2$ formation is also included in Table 3; it serves as an interesting tracer for R_{10} . The differential equations are easily generated by referring to Table 2. Note, however, that H^+ is omitted from all rate expressions and R_{1a} and R_{1b} on Figure 1 have been combined to an overall reaction in Table 2. The differential equations for NADH, $\text{O}_{2(\text{aq})}$, and NAD^+ all have five terms each; Per^{4+} and Per^{6+} have two terms; $(\text{NAD})_2$ has one term; and all others have three terms each. As expected, NADH and $\text{O}_{2(\text{aq})}$ are key dynamical species. It is important to realize that the inclusion of just one additional term in the expression for NAD^+ , specifically $-2k_{10}[\text{NAD}^+]^2$, is the only difference between oscillatory failure (Figure 4a) and success (Figure 4b).

Figure 5 directly compares numerical oxygen and NADH data from the *Urbanalator* with the corresponding experimental data taken under standard conditions of continuous illumination by the deuterium lamp in the spectrophotometer.⁸ Periods and amplitudes are similar, but the induction time (time to the first minimum) is much shorter in the numerical data compared to experiment. Also, the rate of NADH accumulation is consider-

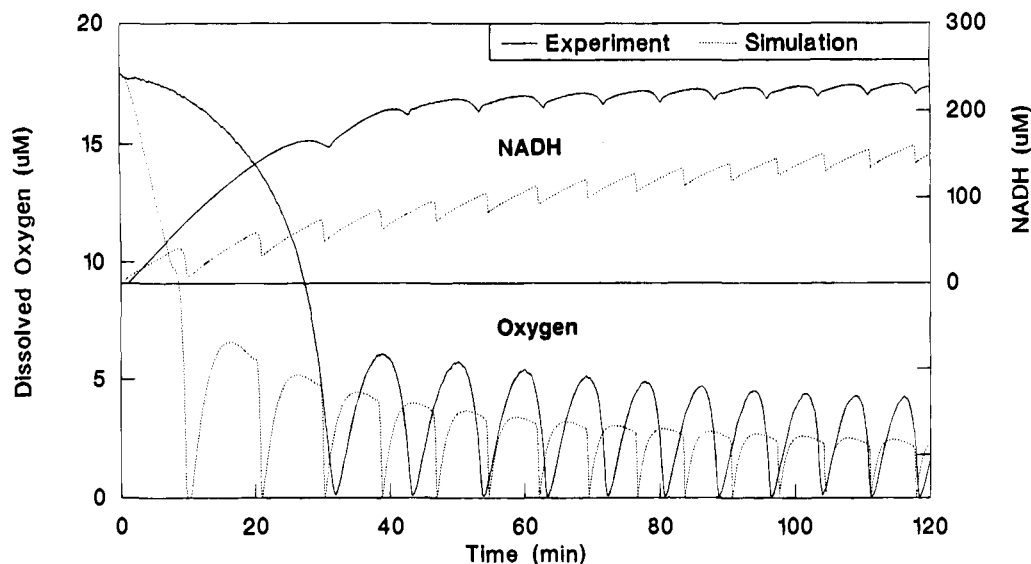


Figure 5. Comparison of standard experimental and simulated data. The experimental traces are excerpted from a previous data set taken under standard conditions.⁸ The conditions for the simulation are for the standard Ubanalator in Tables 2 and 3. Both data sets appear in 10 s intervals.

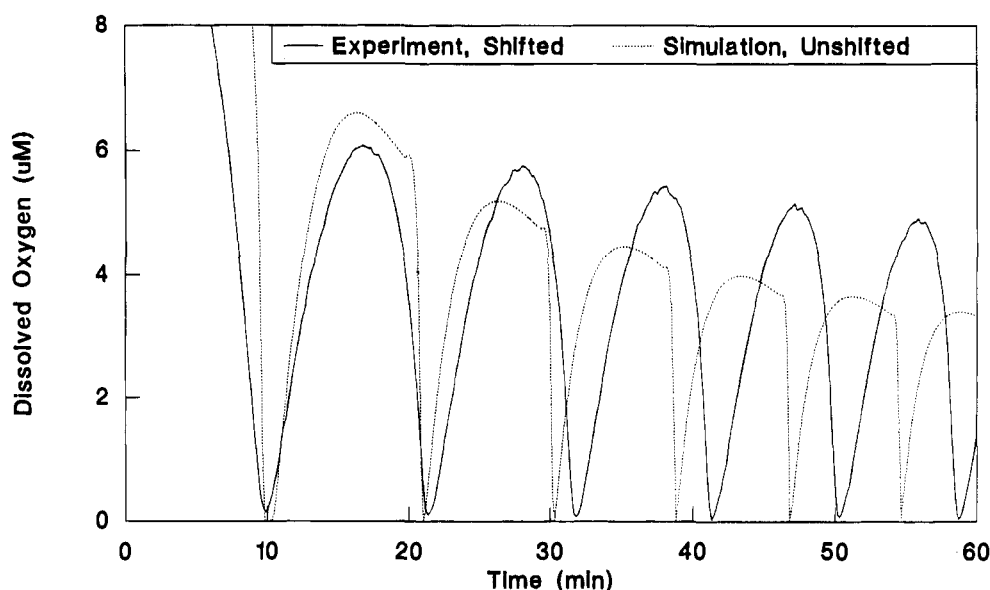


Figure 6. Overlaid experimental and simulated oxygen data. The data from Figure 5 are presented where the first minimum of the simulated data has been shifted to align with the first minimum of the experimental data. All data were taken at 10 s intervals.

ably faster in the experimental run, indicating less NADH consumption than in the simulation. In Figure 6, the first experimental oxygen minimum was shifted to coincide in time with the first minimum in the simulation. The simulated amplitudes and periods both damp faster. This is exactly the opposite of that expected if it is assumed that excess NADH is the cause of this damping.

The amplitude difference of the first oxygen peak in the simulated and experimental data in Figure 6 is within the experimental error for replicates.⁹ The range in the amplitude of the first $O_{2(aq)}$ peak in replicates is about $0.5 \mu\text{M}$. Furthermore, the relative standard deviation (rsd) in the first period ($O_{2(aq)}$ minimum to minimum) of a series of 18 experimental oscillatory runs was nearly 18%. The induction period of about 10 min in the model, however, is distinctly shorter compared to the experimental average of about 30 min ($\pm 17\%$ rsd) for replicate oscillatory runs. The experimental oxygen data in Figure 6 are excerpted from a standard run from previous work.⁸ No attempt was made to find a perfect experimental match to the simulated data in Figure 6; the experimental $O_{2(aq)}$ trace presented there is entirely typical.

Figure 7 compares the experimental and simulated Per^{3+} and Per^{6+} . The experimental enzyme concentrations for these two oxidation states were deconvolved using the respective molar absorptivities at the absorbance maxima of 402 and 418 nm, as explained earlier. Again, the difference in induction times is readily evident. In addition, though these data are qualitatively similar, the excursions of both enzyme states in the model occur across almost the full range allowed by mass balance: about 0.05 to $7.85 \mu\text{M}$. Recall that the deconvoluted spectroscopic data in Figure 2 indicated that the interconversion of Per^{3+} and Per^{6+} might be incomplete. However, since both Per^{3+} and Per^{6+} show a series of minima which are constant for the first 4 h, this suggests a background absorbance which the deconvolution has not taken into account. If this apparent background absorbance could be characterized, the experimental enzyme data might take full excursions similar to those seen in the standard simulation (Figure 7).

Simulated oxygen and Per^{3+} data are shown in Figure 8a. As seen experimentally,⁸ the native enzyme slowly disappears as the oxygen level rises, but then rapidly reappears once the oxygen level falls to near zero. Though the oxygen amplitudes

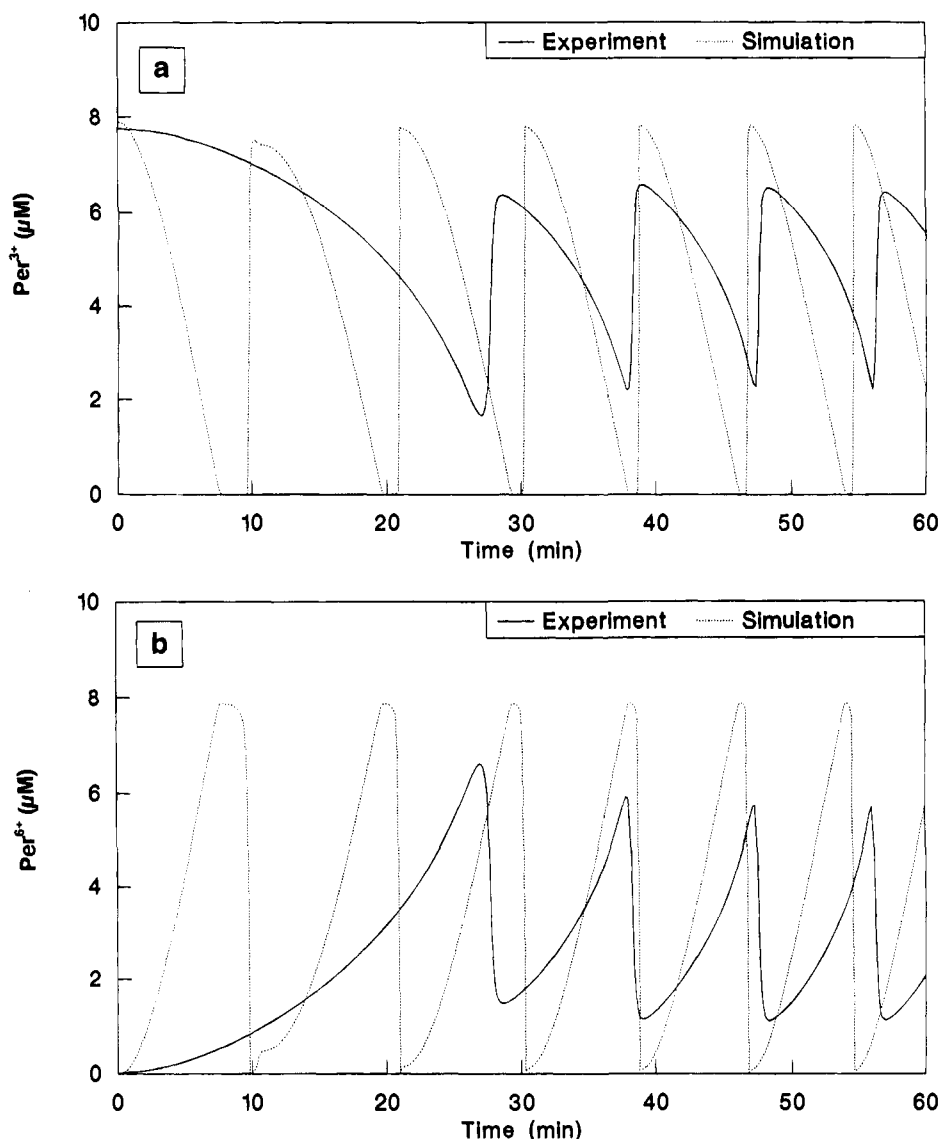


Figure 7. Overlaid experimental and simulated data for Per^{3+} (a) and Per^{6+} (b). The enzyme data from experiment are excerpted from the deconvoluted data in Figure 2a. Simulated data are from the Urbanalator. The time interval is 10 s.

are damped, the Per^{3+} peaks are not. In the Urbanalator, Per^{3+} and Per^{6+} nearly totally interchange with each oscillation.

Oxygen and Per^{4+} are compared in Figure 8b. The Per^{4+} is seen as a brief spike nearly coinciding with the oxygen minimum, indicating rapid formation and depletion of this intermediate. Similar spikes for Per^{5+} are not shown because they are nearly identical. The simulated behavior of both Per^{4+} and Per^{5+} is in agreement with the earlier suggestion from experimental data of a clean interconversion between Per^{3+} and Per^{6+} , as discussed in relation to Figures 2 and 3. The rapid rate of the two reactions which correspond to the consumption of Per^{5+} and Per^{4+} (R_{3a} and R_{3b}) is no doubt driven by the relatively large concentration of NADH.

Numerical artifacts sometimes arise for fine oscillatory features when simulated data are linearly interpolated to yield constant time intervals. For Figure 8b, the output at all the integration steps is displayed (step interval = 1 in HAVCHM), and linear interpolation for output at constant time intervals was not used. These somewhat symmetric spikes have about a 10 s baseline width and a 2 s half-width and are usually composed of 50–60 integration points each. Generation of linearly interpolated data yields irregular peak heights for both Per^{4+} and Per^{5+} . Caution must be taken when such fine features of numerical output are examined. Data should always be initially

computed and viewed at maximum density (minimum step error) and without interpolation (step interval = 1). Interpolated numerical data presented here were generated for ease of comparison using a spreadsheet, but they appear the same when interpolation is not used.

Figure 9 shows the remaining species of interest in the Urbanalator. Since some species appear as spikes, as with Figure 8b, linear interpolation of the simulated output was not used. The free radical species, not surprisingly, are short-lived. Less obvious are the spikes in the appearance of H_2O_2 , which apparently arise when Per^{3+} is momentarily depleted, and Per^{3+} is unable to react with H_2O_2 . $(\text{NAD})_2$ is a non-reactive product in the model and serves as a tracer for R_{10} , merely showing a step of dimer formation at each oxygen minimum. The significance of the peak heights, or of any pattern in them for the radical species shown in Figure 9 or for Per^{4+} and Per^{5+} , is presently unknown. Since the integration routine takes steps constant in error, and the resolving ability of the integration algorithm is uncharacterized in this study, the fine features of the plots will need careful consideration in the future.

The Urbanalator as an Enzyme-Mediated Chemical Switch. Figure 4b showed the effect of varying k_{5a} and hints at the possibility that R_{5a} and R_{5b} combine to govern the shape of oxygen oscillations. The role of R_{5a} and R_{5b} in the

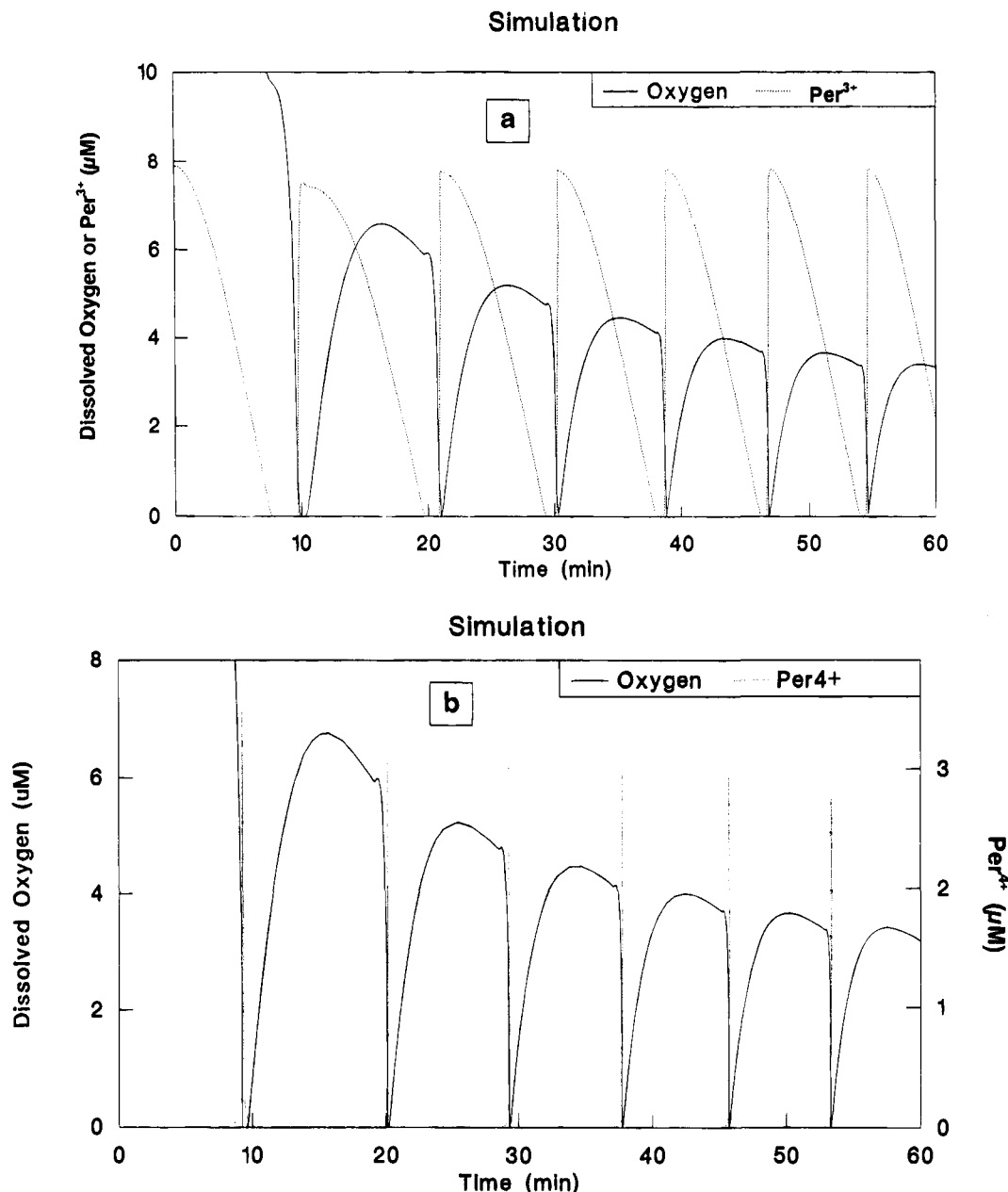


Figure 8. (a) Simulated oxygen and Per^{3+} data from the Urbanalator. The time interval is 10 s. (b) Simulated oxygen and Per^{4+} data from the Urbanalator. Because of the transient nature of the Per^{4+} spikes, data were taken at intervals of constant integration step error but irregular time intervals. See the text for more discussion on numerical artifacts. Otherwise, standard conditions. The Per^{4+} spike begins to rise at the onset of the tiny peak on the oxygen shoulder.

Urbanalator and their function as a chemical switch can be convincingly demonstrated using several approaches.

Varying the values of k_{5a} and k_{5b} (by factors of 10 and 100) in the Urbanalator and examining the resultant oxygen data reveals that these two rate constants affect the shape and amplitude of oxygen oscillations. Furthermore, k_{5a} affects the increasing portion of the oxygen oscillation, and k_{5b} affects the decreasing portion of the peak. Together, the actions of R_{5a} and R_{5b} combine, along with the remainder of the model, to produce a complete oscillation as illustrated in Figure 10a.

To investigate the specific roles of R_{5a} and R_{5b} , an examination of the status of these two reactions, and the effect of that status on oscillations, was undertaken. The upper trace in Figure 10b shows a standard model run through the 6th oxygen minimum. At that point (marked **A**), the numerical value of each species in the oscillator was manually extracted and transferred to become the initial conditions for a new simulation,

but one in which R_{5a} was switched off by setting $k_{5a} = 0$. The new simulation was run, and the resultant data sets were then linked together on a spreadsheet for display. The box on the right side of Figure 10b shows the status of R_{5a} and R_{5b} where OFF means that the corresponding rate constant is set to zero and ON means the constant is set to the standard value on Table 2. In the upper trace, oscillations cease at the oxygen minimum (except for one small peak) because R_{5a} is off, even though R_{5b} is on. If R_{5a} is turned back on at **A** in the 2nd trace (which is precisely the same point as **A** in the first trace), but R_{5b} is shut off, the oxygen rise proceeds normally until it reaches point **B**, where it takes an irregular excursion before returning to the baseline; then, the pattern repeats. At point **B** in the 3rd trace, the status of the switches is reversed and the oxygen decrease proceeds normally, but since R_{5a} is off, oxygen remains at the baseline. When both reactions are returned to their original status, normal behavior resumes and both sides of the oxygen

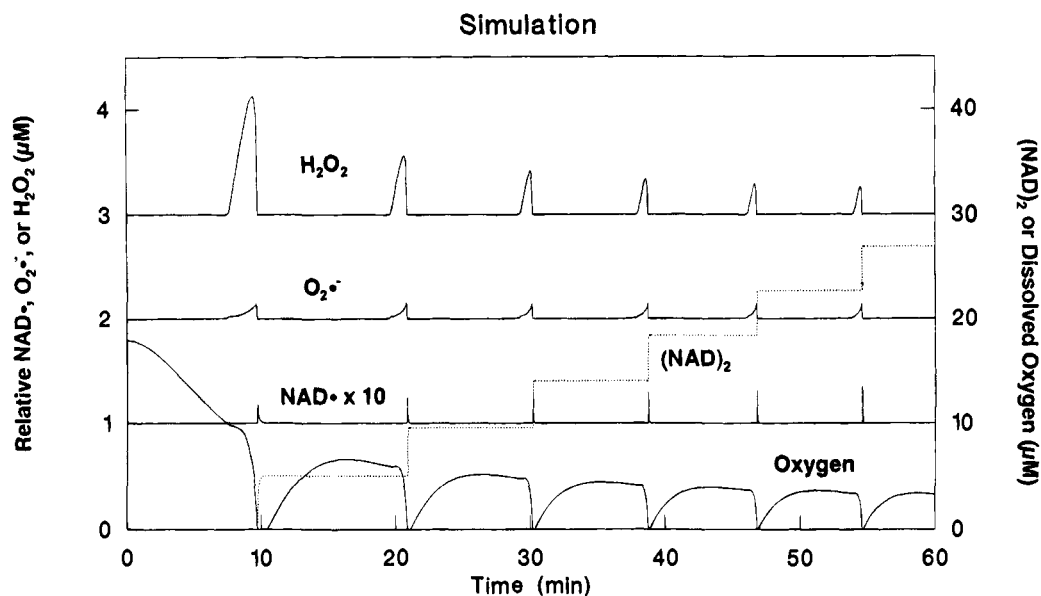


Figure 9. Simulated data for assorted species in the Urbanalator. As in Figure 8b, data were acquired at intervals of constant integration error and not at constant time intervals. NAD^\bullet , $\text{O}_2^{\bullet-}$, and H_2O_2 are offset 1, 2, and 3 μM , respectively, for clarity.

peaks look normal. The action of R_{5a} and R_{5b} in the model as a chemical toggle switch is clearly seen in the box in Figure 10b. The switching point marked by **B** is in the same location as the onset of the tiny bump observed on the right shoulder of the early oxygen oscillations.

The rates of R_{5a} and R_{5b} in the Urbanalator were more closely examined to study their behavior during the course of oscillations. The rate is $k_{5a}[\text{Per}^{3+}][\text{O}_2^{\bullet-}]$ for R_{5a} and $k_{5b}[\text{O}_2^{\bullet-}]^2$ for R_{5b} . Since the numerical integration program generates concentrations for all species at every point, the rates at any point can be directly computed.

Figure 11 displays the ratio of these rates, but normalized against the respective maximum rate to more readily discern the dominant reaction at any given instant. The 6th minimum which appeared at about 54 min was redefined as $t = 0$ in Figure 11. Also, the simulated oxygen data are superimposed on the ratios. Obviously a great deal is happening at the oxygen minima. The rate for R_{5a} is at its maximum near the oxygen minimum, and gradually falls to zero as the oxygen level rises. After oxygen has passed through a maximum, and once Per^{3+} has been exhausted, the R_{5b} rate suddenly increases and quickly reaches its maximum. The oxygen level plummets, R_{5b} shuts off, and R_{5a} comes back on to restart the cycle. R_{5b} is on for only 12% of the period of the oscillation. The switching between R_{5a} and R_{5b} performed manually in Figure 10b is easily seen in detail, as performed by the model alone, in Figure 11.

A physical analogy to the peroxidase-NADH oscillator, termed the siphon model, was proposed in 1973 from experiments conducted earlier.^{42,43} This was neither a numerical nor a comprehensive chemical model, and therefore it could not be compared to experimental data. The approach, however, involves switching events somewhat similar to those described here. An oscillation was divided into three states beginning at the oxygen minimum: inductive (State 1), active (State 2), and terminating (State 3). States similar to these can be defined in the Urbanalator as well and described in more detail. State 1 is the induction phase characterized by a rising oxygen level.

In the Urbanalator, this corresponds to the region dominated by R_{5a} as shown in Figure 11. NADH oxidation and oxygen consumption are increasingly retarded during this phase due to a decreasing amount of Per^{3+} present. Per^{3+} is being converted to Per^{6+} directly by $\text{O}_2^{\bullet-}$ (R_{5a}) and indirectly by NAD^\bullet (R_4 , which in turn produces NAD^\bullet and $\text{O}_2^{\bullet-}$). The most dramatic changes occur during State 2, the active phase. In the Urbanalator, this begins when Per^{3+} is exhausted, R_{5a} virtually ceases, R_{5b} turns on, and excess NAD^\bullet produced by R_{3a} and R_{3b} rapidly consumes oxygen in a free radical burst (readily observed in Figure 9). When Per^{3+} is depleted, R_{5b} becomes rate limiting with respect to R_4 , which slows the reaction of NAD^\bullet with oxygen. This allows excess NAD^\bullet to reduce Per^{6+} via R_6 and, in turn, initiate the rapid cascade of reactions that convert Per^{6+} to Per^{3+} . The active phase is probably best defined as ending when the rate of R_{5a} becomes significantly non-zero. This event begins the termination phase which completes the inactivation of R_{5b} and the exhaustion of oxygen, which coincides with the exhaustion of Per^{6+} and replenishment of Per^{3+} to begin another oscillation.

Future Modification and Applications of the Present Model. The standard Urbanalator in Table 2 is presently a minimal model, including only those reactions deemed necessary to support the interconversion of Per^{3+} and Per^{6+} , and the formation of $(\text{NAD})_2$. It could perhaps be made more complete by inclusion of one or a number of additional chemical reactions. Such alterations might result in better quantitative agreement between simulated and experimental data. A number of possible reactions could be considered based on the literature but not directly on our present experiments. Future work will include the design of experiments which test the inclusion of new reactions to yield a better model. Furthermore, the observed oscillatory damping (Figure 2a); perturbations to the system via addition of MB^+ , catalase, or superoxide dismutase; exposure to light; and comparison of these experiments with analogous numerical simulations are reported elsewhere.⁴⁴

It should be noted that $(\text{NAD})_2$ has a complex chemistry and is actually a mixture of three diastereomers.⁴⁵ In addition, Per^{3+}

(42) Yamazaki, I.; Yokota, K. *Biochim. Biophys. Acta* **1967**, *132*, 310–320.

(43) Yamazaki, I.; Yokota, K. *Biological and Biochemical Oscillators*; Chance, B., Pye, E. K., Ghosh, A. K., Hess, B., Eds.; Academic Press: New York, 1973.

(44) Olson, D. L.; Scheeline, A. Submitted to *J. Phys. Chem.* December 1994.

(45) Carelli, V.; Liberatore, F.; Casini, A.; Mondelli, R.; Arnone, A.; Carelli, I.; Rotilio, G.; Mavelli, I. *Bioorg. Chem.* **1980**, *9*, 342–351.

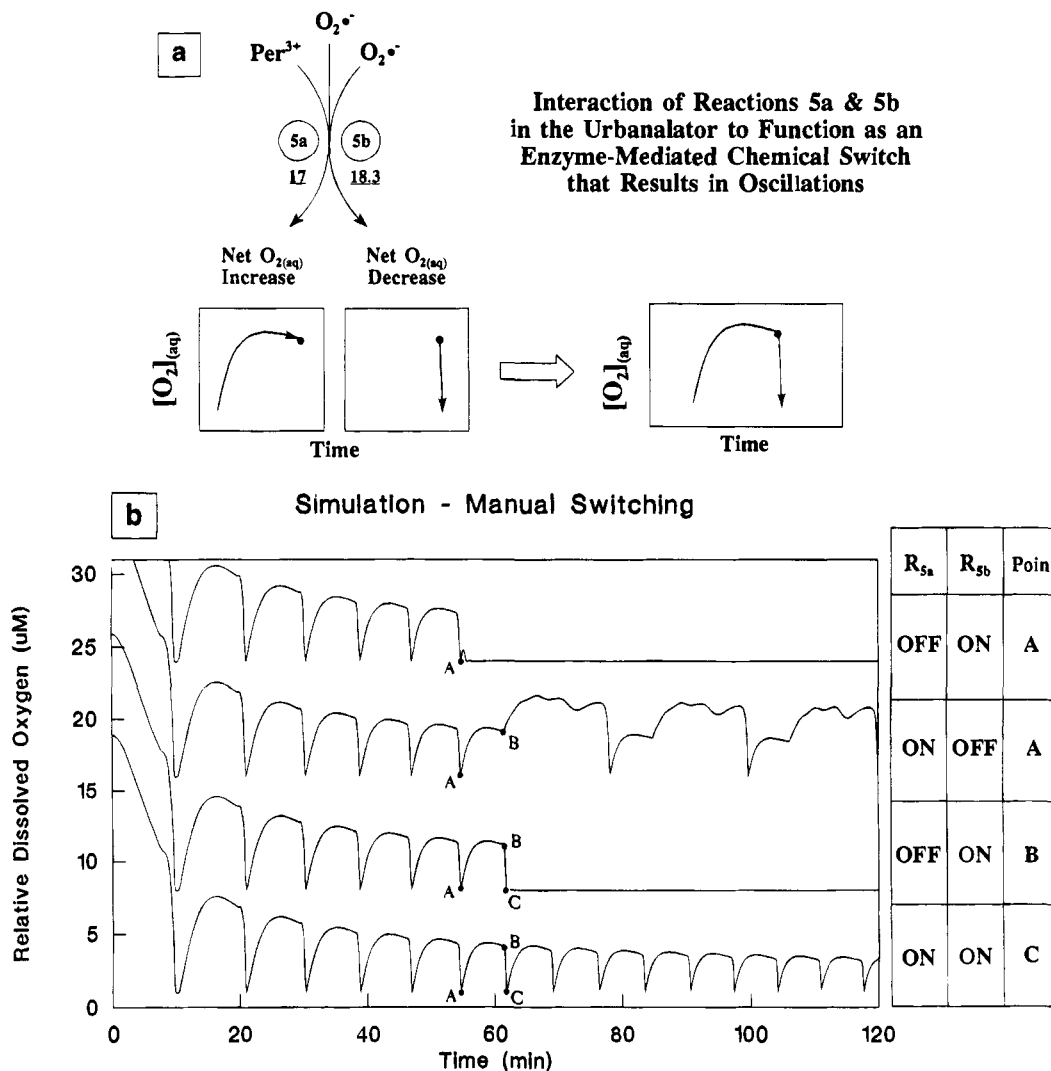


Figure 10. (a) The Urbanalator as an enzyme-mediated chemical switch. Summary illustrating how the interaction of R_{5a} and R_{5b} functions as a chemical switch based on the interconversion of Per^{3+} and Per^{6+} . The relation between the reactions, the general appearance of oxygen data, and how this combines to form an oscillation is depicted. The dominance of R_{5a} switches to R_{5b} when Per^{3+} is depleted. The reverse occurs when Per^{6+} is depleted. (b) Manual switching of R_{5a} and R_{5b} in the Urbanalator. To demonstrate the toggling between these two reactions, switching was performed manually by transferring data generated under one set of switch settings into the initial conditions of another numerical run, but with different switch settings. The four cases are shown in the box at right. Each marked point represents identical data for all species in the model, but with the switch setting changed as shown. ON means the value of the corresponding rate constant has the value from Figure 1. OFF means that the constant is set to zero. Only when both reactions are ON does the simulation generate continuous oscillations.

catalyzes the oxidation and peroxidation of $(\text{NAD})_2$.⁴⁶ The Urbanalator does not include these reactions; R_{10} in the Urbanalator assumes that $(\text{NAD})_2$ is unreactive. The commercially stated purity of the HRP used here is 90% isoenzyme C (Boehringer Mannheim, Indianapolis, IN). The remainder is probably isoenzyme A.⁴⁷ The difference in reactivity of these isoenzymes has not been explored and is not included in the Urbanalator. Despite omission of numerous complicating considerations, the relatively simple, minimal model, presented as the Urbanalator in Figure 1 and Table 2, produces numerical data quite similar to experiments under the conditions discussed here.

Many researchers have used 2,4-dichlorophenol (DCP) in the peroxidase-NADH system, in addition to MB^+ , to stabilize oscillations (see review in ref 8). We found that prolonged, but damped oscillations could be obtained without DCP, which has never been included in any model due to a lack of

knowledge of its reactivity. Its oxidation product could be 2-chloro-1,4-dibenzoquinone⁴⁸ and it may be recycled in the oscillator. Often when DCP was used by others, it was (unnecessarily) dissolved in ethanol. This raises the question as to whether period doubling and chaotic behavior induced by DCP/ethanol additions (32 μM DCP, 27 mM ethanol)^{5,6,8} is actually due to ethanol, even though the effects were attributed to DCP. It would be possible to include the chemistry of DCP and ethanol in the model to search for period doubling or chaotic conditions and compare them to corresponding experiments. However, a better knowledge of the reactivity of these components in the peroxidase-NADH system is required. Various parameters in the present Urbanalator could be varied to search for a variety of oscillatory behaviors, perhaps even without MB^+ .

The experimental approach employed here and previously⁸⁻¹⁰ is based on a semibatch reactor, so termed because oxygen and NADH are supplied from outside the reaction system. Oxygen is continuously allowed to exchange with the outside, but

(46) Avigliano, L.; Carelli, V.; Casini, A.; Finnazzi-Agro, A.; Liberatore, F. *Biochem. J.* **1985**, *226*, 391-375.

(47) Shannon, L. M.; Kay, E.; Lew, J. Y. *J. Biol. Chem.* **1966**, *241*, 2166-2172.

(48) Valli, K.; Gold, M. H. *J. Bacteriol.* **1991**, *173*, 345-352.

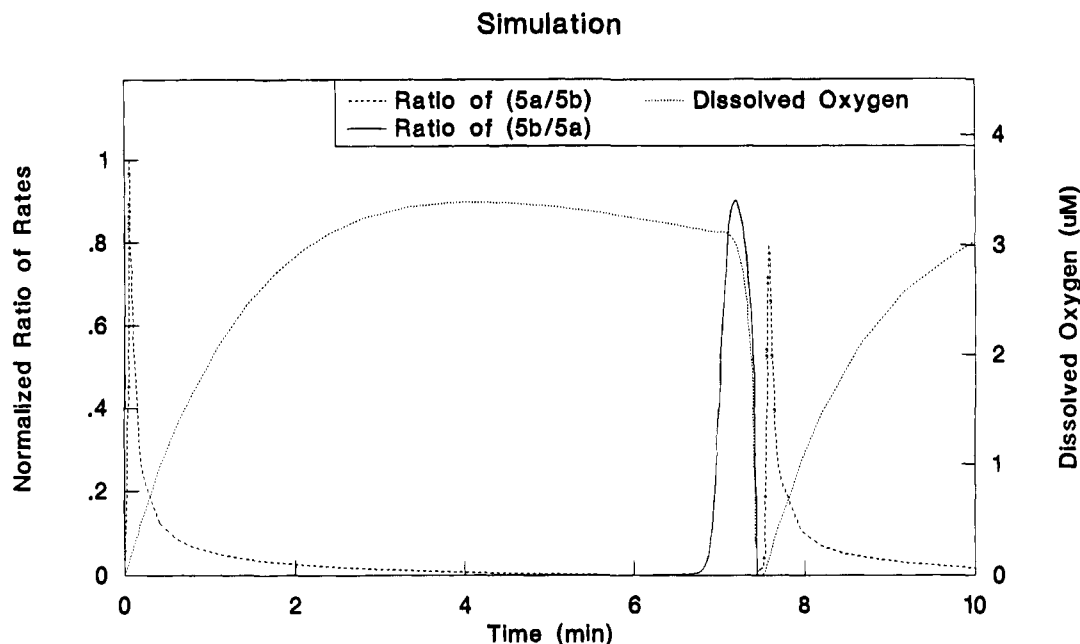


Figure 11. Normalized ratios of rates and oxygen data in the Urbanalator. The oscillation that began at point A in Figure 10b appears at $t = 0$ and C appears at about 7.4 min. The rate for R_{5a} is $k_{5a}[\text{Per}^{3+}][\text{O}_2^{*-}]$; the rate for R_{5b} is $k_{5b}[\text{O}_2^{*-}]^2$. Both were normalized vs their respective maximum in the shown region. Data were generated at intervals of constant integration error. At about 7 min, R_{5b} turns on for approximately 50 s. Before R_{5b} turns completely off, the activation of R_{5a} begins and is complete in about 18 s. Conditions are for the standard Urbanalator.

NADH, HRP, MB^+ , and their various forms are not. This approach was chosen because of its chemical simplicity. Another means to study the peroxidase-NADH oscillator is to use a continuous-flow, stirred tank reactor (CSTR).^{12–15} This requires reactants to be continuously added and withdrawn, but it also requires modification of the chemistry of the oscillatory system. An additional enzyme, glucose-6-phosphate dehydrogenase, is added to recycle NAD^+ to NADH so that continuous NADH influx is not needed. The CSTR approach also includes addition of the enzyme substrate, glucose-6-phosphate, and the formation of its reaction product, 6-phosphogluconolactone. The possible feedback loop created by the addition of three additional chemicals for the CSTR method (suggested by data in ref 1) has not been investigated, but it could be explored using the Urbanalator if appropriate rate constants are available or can be estimated.

The improved, experimentally based understanding of the enzyme-mediated chemical switch presented here opens some interesting possibilities. In a recent study, a switch-like computer model of a biochemical metabolic pathway was created.⁴⁹ It was suggested that such kinetic studies could be used to search for new drug design targets.^{49,50} Perhaps both the experimental and numerical peroxidase-NADH oscillator could be expanded or modified into a more metabolic-like system to serve as a model for the study of switching behavior in biochemical pathways.

Conclusions

It has been demonstrated that the chemically realistic Urbanalator model for the peroxidase-NADH oscillator successfully produces oscillatory results similar to our experimental data, with a minor adjustment in just one literature rate constant. The model consists of 13 steps including oxygen mass transport, NADH delivery, NADH autodegradation, and rate constants taken or derived directly from the literature. Standard experi-

mental data are numerically simulated and in good agreement with the experimentally measured O_2 , NADH, Per^{3+} , and Per^{6+} . Parameter scaling,^{51,52} dimensionless systems and abstract variables with arbitrary rate constants,^{7,16,37,53–58} unidentified species,⁴ or unusual computer requirements are all unnecessary. Unlike many early attempts,¹¹ the enzyme is included in the model. In addition, in building the model, no deliberate attempt was made to specifically include enzymatic feedback control using product activation or substrate inhibition.⁵⁹ The Urbanalator yields results in agreement with earlier predictions¹ that the recycling of Per^{6+} is essential to the observed system periodicity and that Per^{6+} is a regulatory intermediate in the oxidation of NADH by oxygen as catalyzed by Per^{3+} . The Urbanalator indicates that the function of this regulatory intermediate gives HRP the ability to turn itself on and off to produce oscillatory behavior.⁴² Figure 10 demonstrates that in the model, R_{5a} and R_{5b} together function as a toggle switch to control oxygen increases and decreases, respectively. R_{5a} and R_{5b} combine in the model to form an enzyme-mediated chemical switch based on superoxide, relative reaction rates, and alternate depletion and recycling of the native enzyme, Per^{3+} . The Urbanalator model also reveals insights about the behavior of species which have yet to be experimentally observed in the peroxidase-NADH oscillator.

The postulated kinetic scheme presented here surely falls short of a complete picture of the chemistry of the peroxidase-NADH

- (51) Aguda, B. D.; Larter, R. *J. Am. Chem. Soc.* **1990**, *112*, 2167–2174.
 (52) Klein, M. L. M. S. Thesis. Purdue University, Indianapolis, IN, 1992.
 (53) Degn, H.; Mayer, D. *Biochim. Biophys. Acta* **1969**, *180*, 291–301.
 (54) Degn, H.; Olsen, L. F.; Perram, J. W. *Ann. N.Y. Acad. Sci.* **1979**, *316*, 623–639.
 (55) Olsen, L. F. *Phys. Lett.* **1983**, *94A*, 454–457.
 (56) Olsen, L. F. *Z. Naturforsch.* **1985**, *40A*, 1283–1288.
 (57) Fed'kina, V. R.; Ataulakhov, F. I.; Bronnikova, T. V. *Theor. Exp. Chem.* **1988**, *24*, 165–172.
 (58) Alexandre, S.; Dunford, H. B. *Biophys. Chem.* **1991**, *40*, 189–195.
 (59) Noyes, R. M. *J. Phys. Chem.* **1990**, *94*, 4404–4412.
 (60) Dolman, D.; Newell, G. A.; Thurlow, M. D.; Dunford, H. B. *Can. J. Biochem.* **1975**, *53*, 495–501.
 (61) Chance, B. *Arch. Biochem.* **1949**, *22*, 224–252.
 (62) Kashem, M. A.; Dunford, H. B. *Biochem. Cell Biol.* **1986**, *64*, 323–327.

(49) Jackson, R. C. *J. Natl. Cancer Inst.* **1993**, *85*, 539–545.

(50) Morrison, P. F.; Dedrick, R. L. *J. Natl. Cancer Inst.* **1993**, *85*, 518–519.

oscillator. However, the Urbanalator has vastly simplified the modeling approach, as it clearly and directly incorporates critical experimental parameters and requires no special computing power. The greatest potential for use of the Urbanalator lies in

(63) Land, E. J.; Swallow, A. J. *Biochim. Biophys. Acta* **1971**, *234*, 34–42.

(64) Sawada, Y.; Yamazaki, I. *Biochim. Biophys. Acta* **1973**, *327*, 257–265.

(65) Olsen, L. F. *Biochim. Biophys. Acta* **1978**, *527*, 212–220.

(66) Rabani, J.; Nielsen, S. O. *J. Phys. Chem.* **1969**, *73*, 3736–3744.

(67) Behar, D.; Czapski, G.; Rabani, J.; Dorfman, L. M.; Schwarz, H. A. *J. Phys. Chem.* **1970**, *74*, 3209–3213.

its role as a working model to function as a link between experiment and theory. The model will remain the topic of continued investigation and development and serve as a helpful guide to future experiments.

Acknowledgment. Thanks is extended to John P. Chesick for initial advice on the use of HAVCHM. The ease of use of this program greatly facilitated this work. We are also grateful to Ewa Kirkor for her helpful critique of this manuscript.

JA9425290